Available online at www.sciencedirect.com
SCIENCE DIRECT®
ELSEVIER
Journal of Sound and Vibration 279 (2005) 285–308
JOURNAL OF SOUND AND VIBRATION
www.elsevier.com/locate/jsvi

Non-linear dynamics of a one-way clutch in belt–pulley systems

Farong Zhu, R.G. Parker*

Department of Mechanical Engineering, The Ohio State University, 206 W. 18th Ave, Columbus, OH 43210-1107, USA

Received 16 May 2003; accepted 4 November 2003

Abstract

One-way clutches are frequently used in the serpentine belt accessory drives of automobiles and heavy vehicles. The clutch plays a role similar to a vibration absorber in order to reduce belt/pulley vibration and noise and increase belt life. This paper analyzes a two-pulley system where the driven pulley has a one-way clutch between the pulley and accessory shaft that engages only for positive relative displacement between these components. The belt is modelled with linear springs that transmit torque from the driving pulley to the accessory pulley. The one-way clutch is modelled as a piecewise linear spring with discontinuous stiffness that separates the driven pulley into two degrees of freedom. The harmonic balance method combined with arclength continuation is employed to illustrate the non-linear dynamic behavior of the one-way clutch and determine the stable and unstable periodic solutions for given parameters. The results are confirmed by numerical integration and the bifurcation software AUTO. At the first primary resonance, most of the responses are aperiodic, including quasiperiodic and chaotic solutions. At the second primary resonance, the peak bends to the left with classical softening non-linearity because clutch disengagement decouples the pulley and the accessory over portions of the response period. The dependence on clutch stiffness, excitation amplitude, and inertia ratio between the pulley and accessory is studied to characterize the non-linear dynamics across a range of conditions.

1. Introduction

Serpentine belts are widely used in automobiles and heavy vehicles to transmit crankshaft power to all the accessories. Noise reduction and increased belt life are major industry concerns that have their roots in system vibration. Periodic engine pulsations from cylinder

*Corresponding author. Tel.: +614-688-3922; fax: +614-292-3163.
E-mail address: parker.242@osu.edu (R.G. Parker).

0022-460X/$ - see front matter © 2003 Elsevier Ltd. All rights reserved.
doi:10.1016/j.jsv.2003.11.031

ignition generate dynamic excitation for the belt drive. This excitation can, especially near resonance, cause large pulley rotations that lead to "chirp" noise from belt–pulley friction, noise from transverse span vibration, belt slip, and premature belt fatigue or bearing failure [1,2]. Serpentine drives typically have a tensioner arm to maintain belt tension as operating conditions change. Several prior studies [3–8] address the dynamics of serpentine systems.

The evolution of modern vehicles has led to increased electrical needs resulting in increased alternator inertias. The alternator is usually the accessory with the largest inertia and is commonly at the heart of observed vibration problems. One-way clutches are effective devices to mitigate these vibration problems, though they have proved useful on other accessories as well [1,2]. There are several types of one-way clutches, and different names are sometimes used (e.g., one-way decouplers, over-running pulleys). These devices are mounted in the load path between the pulley and the accessory shaft that the pulley drives. In industry, fans in some mechanical systems are equipped with one-way (or over-running) clutches that consist of a ring, hub, rollers and springs. For helicopters, sprag-type over-running clutches are used on the main rotor. Wrap-spring clutches are another design. Different types of one-way clutches perform essentially the same function, namely that of decoupling pulley rotations in the non-driven direction caused by pulley vibrations from rotations of the driven shaft. In essence, the pulley and driven shaft are allowed to rotate relative to each other when the clutch disengages.

One one-way clutch design engages or disengages based on the relative angular speed between the pulley and the accessory shaft. When the accessory pulley decelerates, the one-way clutch disengages, and the accessory rotates freely from the pulley. Because of its greater inertia, however, its deceleration is lower than that of the pulley. When the dynamics of the belt drive system cause the pulley to accelerate, the pulley and accessory remain disengaged until the pulley speed equals that of the accessory. At this point, the one-way clutch engages the accessory and the two rotate together (presuming infinite clutch stiffness) until the pulley again decelerates [2]. This decoupling of the accessory inertia during large vibrations limits belt slip on the pulley.

The clutch design studied in this paper is based on relative displacement between the pulley and accessory. When pulley rotation exceeds accessory shaft rotation, the clutch is engaged with a finite rotational stiffness between the elements. This is the normal driving case. In the opposite case, the clutch disengages and there is no mechanical link between pulley and accessory. This operation is achieved, as one example, with a wrap-spring clutch design. The wrap-spring ends are connected to the pulley and accessory. For positive relative rotation, uncoiling of the spring expands its diameter, creating dry friction on a mating cylinder that couples the pulley and accessory. Negative relative rotation contracts the diameter, releasing the friction and the link between elements.

Though applications of one-way clutches are extensive, literature on their dynamics is limited. Vernay et al. [9] presented an experimental study of sprag-type clutches used in the air turbine starters of jet engines. The clutch is composed of sprags, mounted between two races, and springs that connect the sprags and ensure contact between the sprags and races. The goal is to identify sliding during engagement. King and Monahan [1] discuss a wrap-spring type clutch and elaborate on its functional details. Solfrank and Kelm [2] describe a model for a whole automobile accessory drive system. As an element of their system, a model for an "overrunning alternator pulley" is introduced. The model consists of a speed-dependent damping and a parallel stiffness element. Leamy and Wasfy [10] studied belt creep on the pulley by considering the friction contact

between the pulleys and the belt using finite element method. Their one-way clutch model is a torque proportional to relative pulley/accessory speed that is active only for torque transmission in a single direction.

This paper concentrates on building and analyzing a mathematical model of a two-pulley belt system equipped with a one-way clutch. To focus on the one-way clutch dynamics, no tensioner is included. The belt is modelled as a linear spring transmitting specified motion of the driving pulley (crankshaft) to the driven (accessory) pulley. The one-way clutch is modelled as a non-linear spring with discontinuous stiffness, that is, zero stiffness for the disengaged clutch and finite, linear stiffness for the engaged clutch. A multi-term harmonic balance method (HBM) is developed based on Fourier expansion of the response and discretization of the fundamental period into time increments. Stability of the calculated periodic solutions is assessed by Floquet analysis. Arclength continuation follows the solution branches to determine the stable and unstable solutions as a parameter changes. The results are confirmed by numerical integration and the bifurcation software AUTO [11]. Numerical integration results showing quasiperiodic and chaotic response are calculated for regions of aperiodic response. The system is analyzed for a range of different parameters (magnitude of the non-linear stiffness, excitation amplitude, ratio of the inertia of the pulley to that of the accessory) to characterize where the one-way clutch works most effectively and when the system operates periodically or aperiodically.

2. Mathematical model of one-way clutch

Based on the physical system of the wrap-spring one-way clutch, the model can be described as follows. When the rotations of the wrap-spring ends (that is, the pulley and the accessory shaft) are such that the pulley rotation exceeds the accessory shaft rotation (positive relative displacement) then the clutch is engaged and the clutch torque satisfies $g = K_d(\theta_p - \theta_a)$. Power transmission occurs from driving to driven pulley. For the alternate case where accessory rotation is less than pulley rotation, the wrap-spring diameter decreases and the clutch disengages; no torque is transmitted. In this work, we examine the impact of this one-way clutch on a two-pulley system (Fig. 1(a)). The driving pulley represents the crankshaft, and its motion is specified as $\theta_{c/s} = A_m \cos \omega T$. In vehicle applications, engine firing pulsations induce periodic fluctuations in crankshaft speed at the firing frequency ω. The driven pulley connected to the accessory has inertia J_p. The one-way clutch is integrated between the accessory pulley with rotation θ_p and the accessory shaft with rotation θ_a. Mathematically, the torque transmitted between the accessory pulley and shaft is (Fig. 1(b))

$$g(\delta\theta) = \begin{cases} K_d\delta\theta, & \delta\theta > 0, \\ 0, & \delta\theta \leqslant 0, \end{cases} \tag{1}$$

where $\delta\theta = \theta_p - \theta_a$. The stiffness of the spring is K_d. The belt is modelled as a discrete spring with stiffness K_b. Steady belt tension and belt speed do not affect the system for this belt model. Energy dissipation is modelled as viscous damping using a modal damping model.

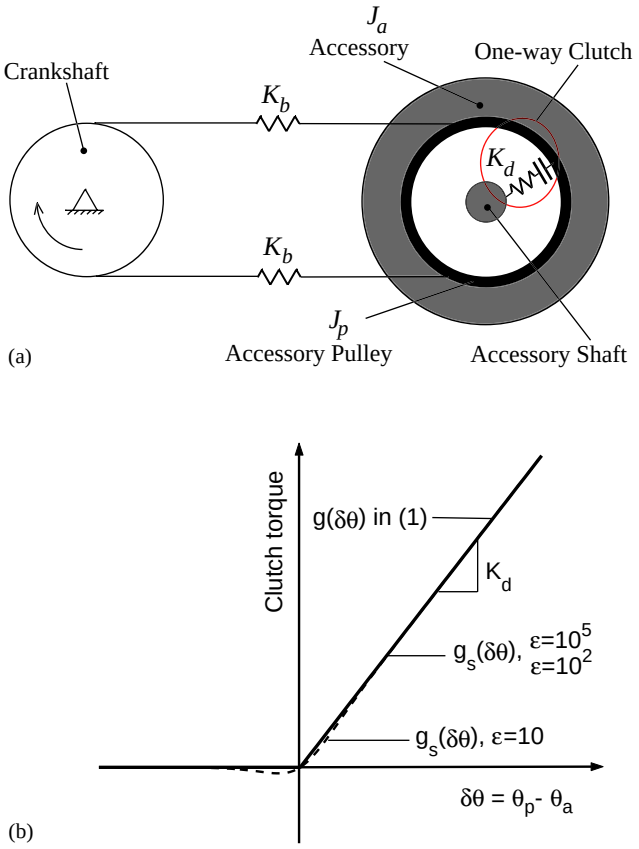

Fig. 1. (a) Two-d.o.f. one-way clutch system; (b) clutch torque $g(\delta\theta)$ in Eq. (1) and the dimensional smoothed function $g_s(\delta\theta)$ according to Eq. (6) for different smoothing parameters ε.

The equations of motion for the pulley and accessory shaft are

$$\begin{aligned} &J_p\ddot{\theta}_p + C_{11}\dot{\theta}_p + C_{12}\dot{\theta}_a + 2K_b r_p^2\theta_p + g(\delta\theta) = M_0 + 2K_b r_p r_{c/s} A_m \cos\omega T,\\ &J_a\ddot{\theta}_a + C_{21}\dot{\theta}_p + C_{22}\dot{\theta}_a - g(\delta\theta) = -M_0, \end{aligned} \tag{2}$$

where r_p, $r_{c/s}$ are the radii of the pulley and the crankshaft. Subscripts p and a refer to the pulley and the accessory, respectively. M_0 is pre-load.

Letting $t = \omega_0 T$, one obtains the dimensionless equations of motion

$$\begin{aligned} &\theta_p'' + \bar{C}_{11}\theta_p' + \bar{C}_{12}\theta_a' + \bar{K}_b\theta_p + \bar{g}(\delta\theta) = \bar{M} + \beta\bar{K}_b A_m \cos\Omega t,\\ &\alpha\theta_a'' + \bar{C}_{21}\theta_p' + \bar{C}_{22}\theta_a' - \bar{g}(\delta\theta) = -\bar{M}, \end{aligned} \tag{3}$$

$$\bar{g}(\delta\theta) = \begin{cases} \bar{K}_d\delta\theta, & \delta\theta > 0,\\ 0, & \delta\theta \leqslant 0, \end{cases} \tag{4}$$

where the dimensionless parameters are

$$\Omega = \frac{\omega}{\omega_0}, \quad \alpha = \frac{J_a}{J_p}, \quad \beta = \frac{r_{c/s}}{r_p}, \quad \bar{K}_b = \frac{2K_b r_p^2}{J_p \omega_0^2}, \quad \bar{K}_d = \frac{K_d}{J_p \omega_0^2}, \quad \bar{M} = \frac{M_0}{J_p \omega_0^2}. \tag{5}$$

The frequency ω_0 is chosen as the natural frequency for the linear system in which the accessory is not equipped with a one-way clutch. In this case it is a single degree of freedom (s.d.o.f.) system and the natural frequency is $\omega_0 = \sqrt{2K_b r_p^2/(J_p + J_a)}$.

The damping matrix $\bar{\mathbf{C}} = \mathbf{V}^{-\mathrm{T}} \operatorname{diag}(2\zeta\Omega_i)\mathbf{V}^{-1}$ is obtained by transforming the modal damping matrix $\operatorname{diag}(2\zeta\Omega_i)$ where ζ is a specified modal damping ratio and $\mathbf{v}_i$, Ω_i are the eigensolutions for the two-d.o.f. linear system with the clutch engaged. Corresponding to this linear system, the dimensionless natural frequencies are $\Omega_1 = 0.982$ and $\Omega_2 = 6.811$ for the values in Table 1. Fig. 2 shows the mode shapes for the linear system. The pulley and accessory rotate in-phase in the first mode and out-of-phase in the second mode.

Fig. 3 shows the root mean square (r.m.s.) of $\delta\theta - \delta\theta_{mean}$ versus excitation frequency for the values $\zeta = 3, 5, 8\%$ obtained by numerical integration for parameter values in Table 1. Increasing and decreasing frequency sweeps are shown. For $\zeta = 8\%$, the branches calculated for increasing and decreasing frequencies overlay each other; the behavior is linear. For $\zeta = 3\%$ and 5%, non-linear jump phenomena occur. These results are sensitive to the excitation amplitude. For the nominal excitation amplitude used in this work (Table 1), we specify 3% modal damping to capture the relatively light damping internal to a one-way clutch and induce the non-linear response exhibited by these systems in practice.

In this paper, multiple methods are employed to address the discontinuous stiffness non-linearity shown in Fig. 1(b). Among these are harmonic balance (HBM) and the bifurcation software AUTO, which requires continuous functions. To approximate $\bar{g}(\delta\theta)$ in Eq. (4) by a smooth function, the hyperbolic tangent function is used according to

$$\bar{g}_s(\delta\theta) = \tfrac{1}{2}\bar{K}_d[1 + \tanh(\varepsilon\delta\theta)]\delta\theta. \tag{6}$$

Fig. 1(b) compares the dimensional clutch torque $g(\delta\theta)$ in Eq. (1) and the smoothed function $g_s(\delta\theta)$ corresponding to Eq. (6). The difference is indistinguishable for large $\varepsilon > 100$. By numerical investigation, Fig. 4 shows the effect of approximating the step function by Eq. (6) with given ε.

Table 1
Parameters for the nominal case

$r_p = 0.028575$ (m)	Radius of pulley
$r_{c/s} = 0.040625$ (m)	Radius of crankshaft
$J_p = 0.001607$ (kg m^2)	Pulley inertia
$\alpha = J_a/J_p = 1.620$	Inertia ratio
$\zeta = 3\%$	Modal damping ratio
$K_b = 2.5 \times 10^5$ (N/m)	Belt stiffness
$K_d = 5000$ (N/rad)	Clutch spring stiffness
$A_m = 0.001$ (rad)	Excitation amplitude
$M_0 = 2.3$ (N m)	Preload

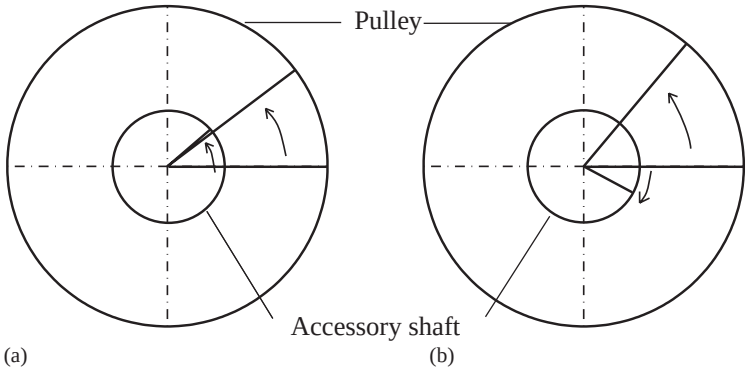

Fig. 2. Vibration modes for the parameters in Table 1: (a) Mode 1, $\Omega_1 = 0.982$; (b) Mode 2, $\Omega_2 = 6.81$.

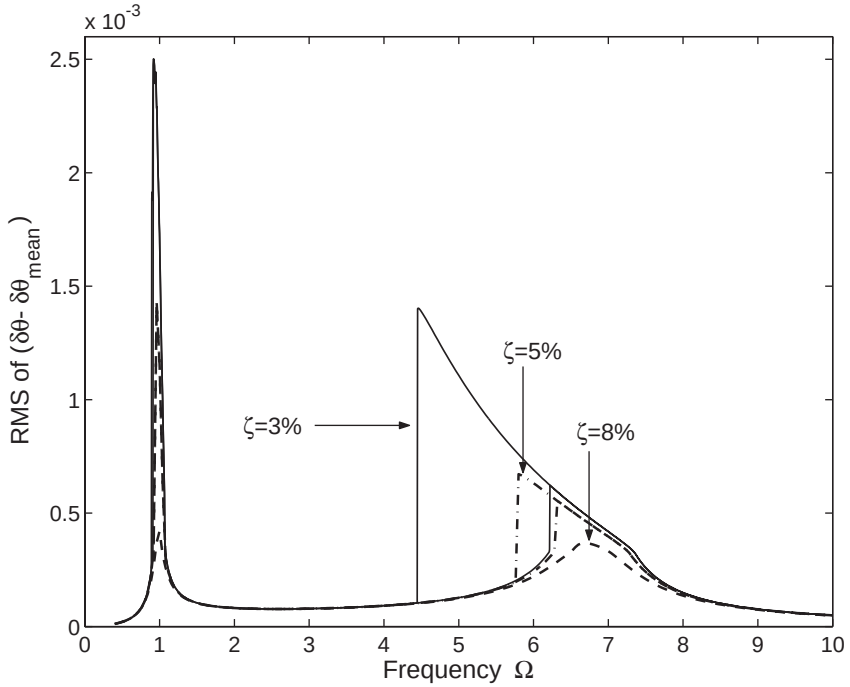

Fig. 3. The r.m.s. of $(\delta\theta - \delta\theta_{mean})$ for modal damping ratios $\zeta = 3, 5, 8\%$ obtained by numerical integration with step function for the clutch torque $\bar{g}(\delta\theta)$ (see Eq. (4)). Parameters are in Table 1.

$\varepsilon > 2000$ produces an acceptable approximation to the step function for this system. The value $\varepsilon = 10\,000$ yields a better approximation and causes no numerical trouble for HBM and AUTO, so this value is used throughout. $\bar{g}_s(\delta\theta)$ replaces $\bar{g}(\delta\theta)$ in subsequent results except where indicated otherwise.

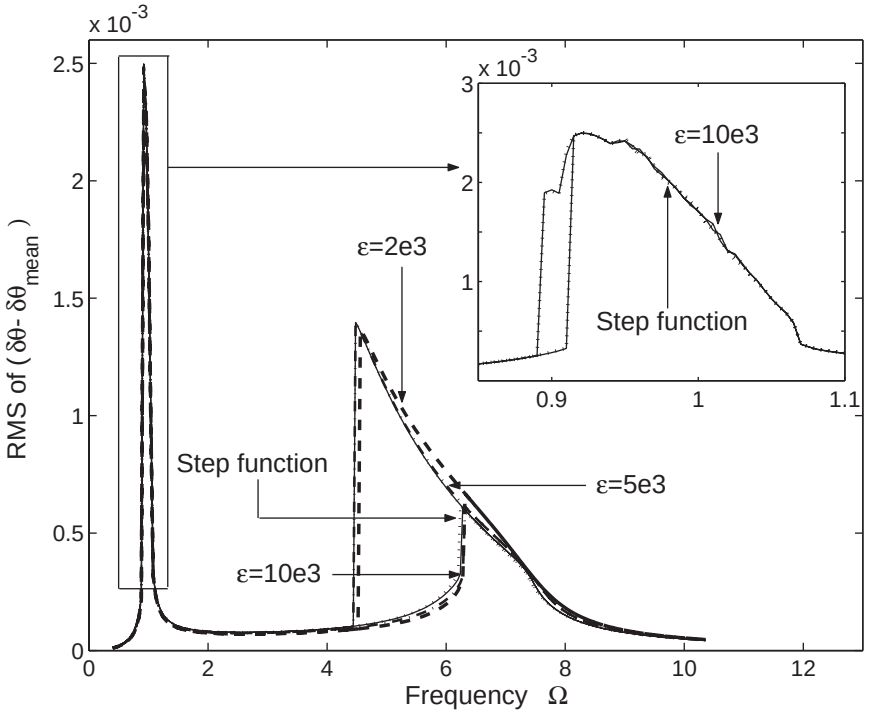

Fig. 4. Dynamic response, r.m.s. of $\delta\theta - \delta\theta_{mean}$, by numerical integration using the step function $\bar{g}(\delta\theta)$ in Eq. (4) and different ε in the approximation $\bar{g}_s(\delta\theta)$ in Eq. (6).

3. HBM with arclength continuation and stability

The harmonic balance method is widely used to seek periodic solutions of non-linear systems, especially those having clearance non-linearity. With the assumption of periodic motion, the variables are expanded by Fourier series so as to map the system from the time domain into the frequency domain to get periodic solutions. By taking a gear pair as an example and applying the standard HBM, Blankenship and Kahraman [12] studied the behavior of a mechanical system exhibiting combined parametric excitation and clearance type non-linearity. Leamy and Perkins [13] utilized the harmonic balance method to investigate the non-linear periodic response of engine accessory drives with dry friction tensioners. Padmanabhan and Singh [14] analyzed periodically excited non-linear systems with an example of a gear pair with discontinuous mesh stiffness by using a parametric continuation technique. Continuation techniques have been used by many researchers for non-linear systems. It is a path following procedure using arclength continuation to trace the bifurcation diagram. By this method, Raghothama and Narayanan [15] studied the bifurcation and chaos in a geared rotor bearing system. Von Groll and Ewins [16] examined rotor/stator interaction dynamics for varying shaft rotation speeds.

Combined with arclength continuation, HBM is effective to examine how the system behavior varies with the system parameters, and this method is adopted in this paper. A brief description of HBM with arclength continuation applied to Eq. (3) with smoothing function (6) is given below.

First, consider the response to be periodic and expand the solution using Fourier series truncated to R harmonics:

$$\theta_p(t) = u_{p,1} + \sum_{r=1}^{R}(u_{p,2r}\cos r\Omega t + u_{p,2r+1}\sin r\Omega t),$$

$$\theta_a(t) = u_{a,1} + \sum_{r=1}^{R}(u_{a,2r}\cos r\Omega t + u_{a,2r+1}\sin r\Omega t). \tag{7}$$

Then, discretize the time domain into N intervals as $t_0, \ldots, t_n, \ldots, t_{N-1}$ and introduce the operator $\mathbf{L}_0$ such that the time-discretized response vector is

$$\mathbf{x}(\mathbf{t}) = \{\theta_p(t_0) \ \cdots \ \theta_p(t_{N-1}) \ \theta_a(t_0) \ \cdots \ \theta_a(t_{N-1})\}^{\mathrm{T}} = \begin{bmatrix} \mathbf{L}_0 & \mathbf{0} \\ \mathbf{0} & \mathbf{L}_0 \end{bmatrix}\mathbf{u} = \mathbf{L}\mathbf{u}, \tag{8}$$

where $\mathbf{u} = \{u_{p,1} \ \cdots \ u_{p,2R+1} \ u_{a,1} \ \cdots \ u_{a,2R+1}\}^{\mathrm{T}}$. Introducing a $(2R+1)\times(2R+1)$ operator $\mathbf{A}_0 = \mathrm{diag}(0, 1^2, 1^2, 2^2, 2^2, \ldots, r^2, r^2, \ldots)$ and a similar operator $\mathbf{B}_0$ and defining

$$\mathbf{A} = (-\Omega^2)\begin{bmatrix} \mathbf{A}_0 & \mathbf{0} \\ \mathbf{0} & \mathbf{A}_0 \end{bmatrix}, \quad \mathbf{B} = \Omega\begin{bmatrix} \mathbf{B}_0 & \mathbf{0} \\ \mathbf{0} & \mathbf{B}_0 \end{bmatrix},$$

one can express $\dot{\mathbf{x}}(\mathbf{t})$ and $\ddot{\mathbf{x}}(\mathbf{t})$ as

$$\dot{\mathbf{x}} = \mathbf{L}\mathbf{B}\mathbf{u}, \quad \ddot{\mathbf{x}} = \mathbf{L}\mathbf{A}\mathbf{u}. \tag{9}$$

The non-linear function $\mathbf{h} = \{\bar{g}_s(\delta\theta), -\bar{g}_s(\delta\theta)\}^{\mathrm{T}}$ and the forcing function $\mathbf{f} = \{\bar{M} + \beta\bar{K}_b A_m \cos\Omega\mathbf{t}, -\bar{M}\}^{\mathrm{T}}$ are similarly expanded in Fourier series as

$$\mathbf{h} = \mathbf{L}\mathbf{d}, \quad \bar{\mathbf{f}} = \mathbf{L}\mathbf{F}. \tag{10}$$

By defining

$$\tilde{\mathbf{m}} = \begin{bmatrix} \mathbf{I} & \mathbf{0} \\ \mathbf{0} & \alpha\mathbf{I} \end{bmatrix}, \quad \tilde{\mathbf{c}} = \begin{bmatrix} \bar{C}_{11}\mathbf{I} & \bar{C}_{12}\mathbf{I} \\ \bar{C}_{21}\mathbf{I} & \bar{C}_{22}\mathbf{I} \end{bmatrix} \quad \text{and} \quad \bar{\mathbf{k}} = \begin{bmatrix} \bar{K}_b\mathbf{I} & \mathbf{0} \\ \mathbf{0} & \mathbf{0} \end{bmatrix},$$

where $\mathbf{I}$ is a $(2R+1)\times(2R+1)$ identity matrix, substitution of Eqs. (8)–(10) into Eq. (3) yields

$$\mathbf{L}[(\tilde{\mathbf{m}}\mathbf{A} + \tilde{\mathbf{c}}\mathbf{B} + \tilde{\mathbf{k}})\mathbf{u} - \mathbf{F} + \mathbf{d}] = \mathbf{L}\mathbf{E} = \mathbf{0},$$

$$\mathbf{E} = \bar{\mathbf{K}}\mathbf{u} - \mathbf{F} + \mathbf{d}, \quad \bar{\mathbf{K}} = \tilde{\mathbf{m}}\mathbf{A} + \tilde{\mathbf{c}}\mathbf{B} + \tilde{\mathbf{k}}. \tag{11}$$

The vector $\mathbf{u}$ that determines $\mathbf{x}$ is found from

$$\mathbf{E} = \mathbf{0}. \tag{12}$$

We seek to follow periodic solution branches as a parameter p of the system changes (such as frequency, where $p = \Omega$). In particular, it is desirable to trace stable and unstable branches in the space of u_i and p, and these branches generally involve curves that reverse direction. Baker and Overman [17] describe a continuation method approach. In this spirit, we introduce the solution branch arclength parameter s as an independent variable and consider the system parameter p as an unknown as well. The residue $\mathbf{E}$ in Eq. (11) then has $2(2R+1)+1$ unknowns

$\bar{\mathbf{u}}(s) = \{\mathbf{u}(s)^{\mathrm{T}} \; p(s)\}^{\mathrm{T}}$ and the infinitesimal arclength $\mathrm{d}s$ satisfies

$$\mathrm{d}s^2 = \sum_{i=1}^{2R+1} \mathrm{d}u_i^2 + \mathrm{d}p^2 \quad \Rightarrow \quad 1 = \sum_{i=1}^{2R+1} \left(\frac{\mathrm{d}u_i}{\mathrm{d}s}\right)^2 + \left(\frac{\mathrm{d}p}{\mathrm{d}s}\right)^2. \tag{13}$$

According to Newton–Raphson iteration,

$$\bar{\mathbf{u}}_{new} = \bar{\mathbf{u}}_{old} - \mathbf{J}|_{\bar{\mathbf{u}}_{old}}^{-1} \mathbf{E}(\bar{\mathbf{u}}_{old}), \tag{14}$$

where the Jacobian matrix is

$$\mathbf{J} = \left[\frac{\partial \mathbf{E}}{\partial \mathbf{u}} \quad \frac{\partial \mathbf{E}}{\partial p}\right], \quad \frac{\partial \mathbf{E}}{\partial \mathbf{u}} = \bar{\mathbf{K}} + \frac{\partial \mathbf{d}}{\partial \mathbf{u}} = \bar{\mathbf{K}} + \mathbf{\Gamma} \frac{\partial \mathbf{h}}{\partial \mathbf{x}} \mathbf{L} \tag{15}$$

and $\mathbf{J}^{-1}$ denotes the pseudo-inverse. We have used

$$\mathbf{d} = \mathbf{\Gamma h} = \begin{bmatrix} \mathbf{\Gamma}_0 & \mathbf{0} \\ \mathbf{0} & \mathbf{\Gamma}_0 \end{bmatrix} \mathbf{h}, \tag{16}$$

where $\mathbf{\Gamma}_0$ represents the discrete Fourier transformation operator with $\Gamma_{0_{1,n}} = 1/N$, $\Gamma_{0_{2r,n}} = (2/N)\cos(2\pi r(n-1)/N)$ and $\Gamma_{0_{2r+1,n}} = (2/N)\sin(2\pi r(n-1)/N)$ for $r = 1, 2, \ldots, R$ and $n = 1, \ldots, N$. iteration continues until $\varepsilon = ||\bar{\mathbf{u}}_{new} - \bar{\mathbf{u}}_{old}||$ is within a specified tolerance.

To improve convergence, it is important to provide an appropriate initial guess for iteration of Eq. (14). For the two-dimensional case, the tangent line of the solution branch at the current solution $\bar{\mathbf{u}}_k(s)$ defines the axis along which the initial guess for the next solution $\bar{\mathbf{u}}_{k+1}(s)$ lies [17]. Generalizing to higher dimensions, Eq. (12) describes $2(2R+1)$ hypersurfaces and the solutions $\bar{\mathbf{u}}(s)$ lie on the intersection of these hypersurfaces. The desired initial guess lies along the axis that is the intersection of the tangent planes of these hypersurfaces at the current solution. Differentiating Eq. (12) at $\bar{\mathbf{u}}_k(s)$,

$$\left.\frac{\partial \mathbf{E}}{\partial \mathbf{u}}\right|_{\bar{\mathbf{u}}_k} \frac{\partial \mathbf{u}}{\partial s} + \left.\frac{\partial \mathbf{E}}{\partial p}\right|_{\bar{\mathbf{u}}_k} \frac{\partial p}{\partial s} = \mathbf{J}|_{\bar{\mathbf{u}}_k} \boldsymbol{\tau} = 0, \tag{17}$$

where $\boldsymbol{\tau} = [\partial \mathbf{u}/\partial s \;\; \partial p/\partial s]^{\mathrm{T}}$. $\mathbf{J}|_{\bar{\mathbf{u}}_k}$ represents the gradients of the surfaces at $\bar{\mathbf{u}}_k(s)$, and $\boldsymbol{\tau}$ is on the intersection of the tangent planes. $\boldsymbol{\tau}$ is a basis of the nullspace of $\mathbf{J}|_{\bar{\mathbf{u}}_k}$ where $\mathbf{J}|_{\bar{\mathbf{u}}_k}$ has rank $2(2R+1)$ except at bifurcation points. Alternatively, $\boldsymbol{\tau}$ is a basis of the left nullspace of $\mathbf{J}|_{\bar{\mathbf{u}}_k}^{\mathrm{T}}$ from $\boldsymbol{\tau}^{\mathrm{T}} \mathbf{J}|_{\bar{\mathbf{u}}_k}^{\mathrm{T}} = \mathbf{0}^{\mathrm{T}}$. From QR decomposition of $\mathbf{J}|_{\bar{\mathbf{u}}_k}^{\mathrm{T}}$, $\mathbf{Q}^{\mathrm{T}} \mathbf{J}|_{\bar{\mathbf{u}}_k}^{\mathrm{T}} = \mathfrak{R}$, where $\mathbf{Q}$ is an orthonormal square matrix and $\mathfrak{R}$ is an upper triangular matrix with zero elements in the last row,

$$\begin{bmatrix} \mathbf{q}_1^{\mathrm{T}} \\ \vdots \\ \mathbf{q}_{2(2R+1)+1}^{\mathrm{T}} \end{bmatrix} \mathbf{J}|_{\bar{\mathbf{u}}_k}^{\mathrm{T}} = \begin{bmatrix} \times & \cdots & \times \\ 0 & \vdots & \vdots \\ \vdots & 0 & \times \\ 0 & \cdots & 0 \end{bmatrix}. \tag{18}$$

Consequently, $\mathbf{q}_{2(2R+1)+1}^{\mathrm{T}} \mathbf{J}|_{\bar{\mathbf{u}}_k}^{\mathrm{T}} = 0^{\mathrm{T}}$, and $\boldsymbol{\tau} = \mathbf{q}_{2(2R+1)+1}$. Orthonormality of $\mathbf{Q}$ implies $||\boldsymbol{\tau}|| = 1$ in accordance with Eq. (13). The sign of $\boldsymbol{\tau}$ must be chosen to ensure the solution path is traced "forward" in the arclength direction. If the inner product $\boldsymbol{\tau}_{k-1}^{\mathrm{T}} \boldsymbol{\tau} < 0$, let $\boldsymbol{\tau}_k = -\boldsymbol{\tau}$, otherwise $\boldsymbol{\tau}_k = \boldsymbol{\tau}$ (subscript k denotes the current solution). Δs_k is determined by step size control [17] and then $\bar{\mathbf{u}}_{k+1}^0 = \bar{\mathbf{u}}_k + \Delta s_k \boldsymbol{\tau}_k$ establishes the initial guess.

To establish the stability of periodic solutions from harmonic balance, much of the literature employs Floquet multipliers [12,14,15,18,19]. Von Groll and Ewins [16] apply Hill's method. Both methods were used here, and we found Floquet multipliers to produce more reliable results for known example problems. When applying Floquet multipliers, Friedmann et al. [20] compared two numerical schemes to obtain the monodromy matrix. One is developed by Hsu [21,22], which has been widely used for stability analysis [12,14,15,18,19]. That idea is to discretize a period into a number of intervals and consider the periodic coefficient matrices to be constant over each interval. The second approach is a numerical integration scheme improved in [20]. It is based on the fourth order Runge–Kutta method and requires less computer time to converge than Hsu's method. Here, numerical integration is employed to find the monodromy matrix, whose eigenvalues $\lambda_i,\ i=1,\ldots,4$ are the Floquet multipliers. The solution stability is classified as follows: if there exists any $||\lambda_i|| > 1$, that eigenvalue (and the solution) is unstable; if all the eigenvalues satisfy $||\lambda_i|| < 1$, the solution is stable.

The values $R = 18$ and $N = 512$ in Eqs. (7) and (8) are used in results to follow. While the shape of the solutions branches is not highly sensitive to R, this number of terms was found to give better stability conclusions than lower values.

In addition to harmonic balance, subsequent results compare findings from numerical integration and the bifurcation software AUTO. AUTO performs bifurcation analysis of systems of the form

$$\mathbf{y}'(t) = \mathbf{f}(\mathbf{y}(t), p), \quad \mathbf{f}(\cdot,\cdot), \mathbf{y}(\cdot) \in \mathbb{R}^n, \tag{19}$$

where p denotes one or more free parameters. AUTO is employed to compute branches of stable and unstable periodic solutions as well as locate bifurcations along these branches.

4. Results

4.1. Excitation frequency sweep

In this section, the nominal case solutions are examined over a range of excitation frequency. In automotive belt drives, the excitation frequency is the engine firing frequency, which varies across a wide range. Fig. 5 shows the steady state (r.m.s.) dynamic amplitude of the relative pulley–accessory rotation $(\theta_p - \theta_a) - (\theta_p - \theta_a)_{mean}$ as the excitation frequency varies. Results for increasing and decreasing frequency are shown. The parameters considered are those in Table 1. For the results from numerical integration, the increasing and decreasing frequency branches coincide except for the resonant regimes near the natural frequencies $\Omega_{1,2} = 0.982, 6.81$ of the linear system corresponding to a clutch of stiffness $\bar{K}_d = 27.66$. Hysteretic behavior corresponding to a softening non-linearity is evident for $\Omega \approx \Omega_2$. The softening behavior is a result of clutch disengagement where the spring between the pulley and accessory shaft is inactive. A slight kink occurs at the transition from clutch engagement at all times (linear system) to frequencies where the clutch disengages during some portion of the periodic solution. Non-linear disengagement occurs outside the range where multiple steady state periodic solutions are possible. The waterfall plots of Fig. 6 show the numerical integration spectra as excitation frequency increases and decreases. The higher harmonics of excitation frequency for $\Omega \approx \Omega_2$ indicate periodic, but not

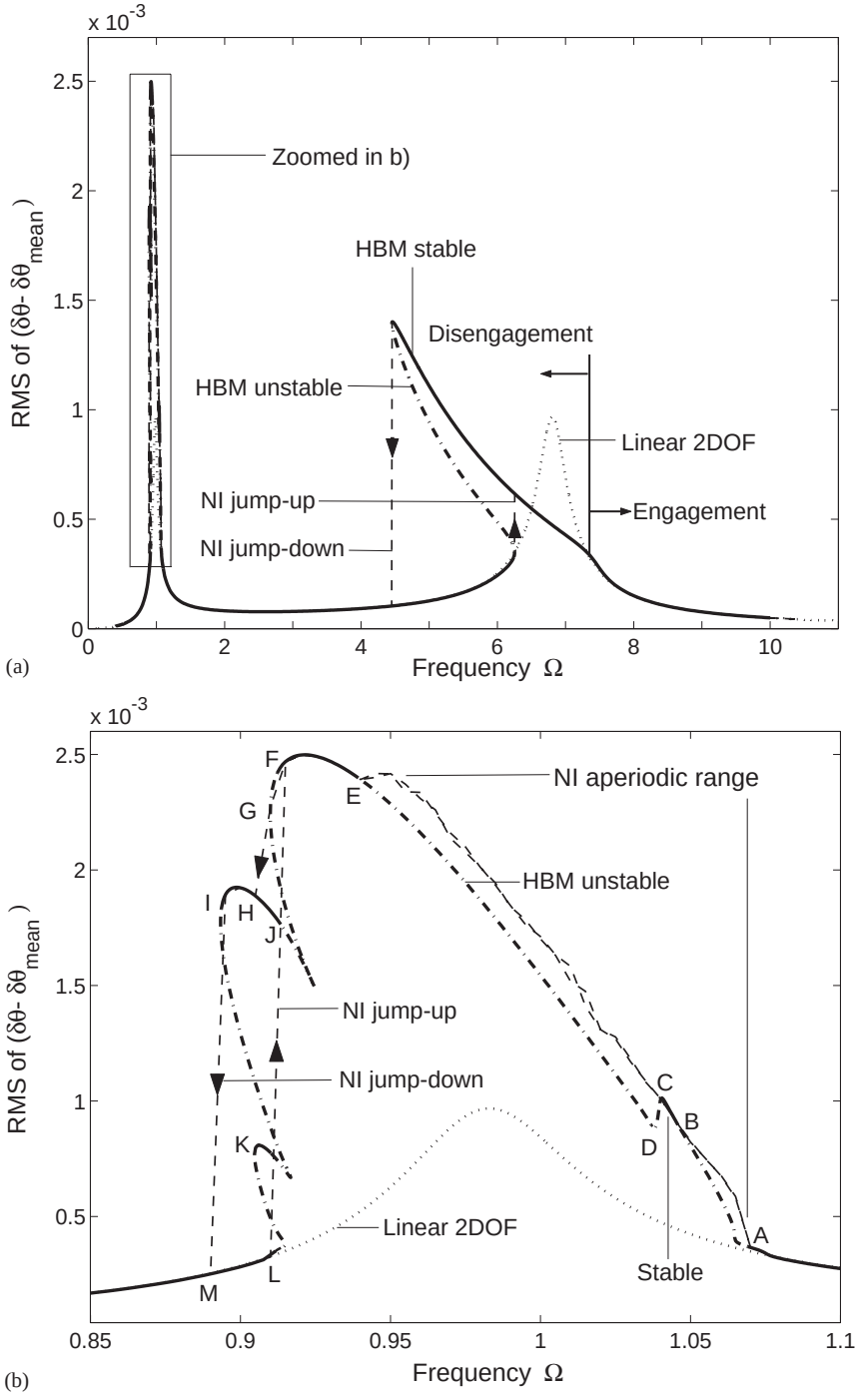

Fig. 5. The r.m.s. of $(\delta\theta - \delta\theta_{mean})$ versus excitation frequency for the nominal case of Table 1: (a) over a range of excitation frequencies including two resonances; (b) zooming (a) at the first resonant region. HBM stable (-), unstable (-·); numerical integration (NI) (- -); two-d.o.f. linear system (..).

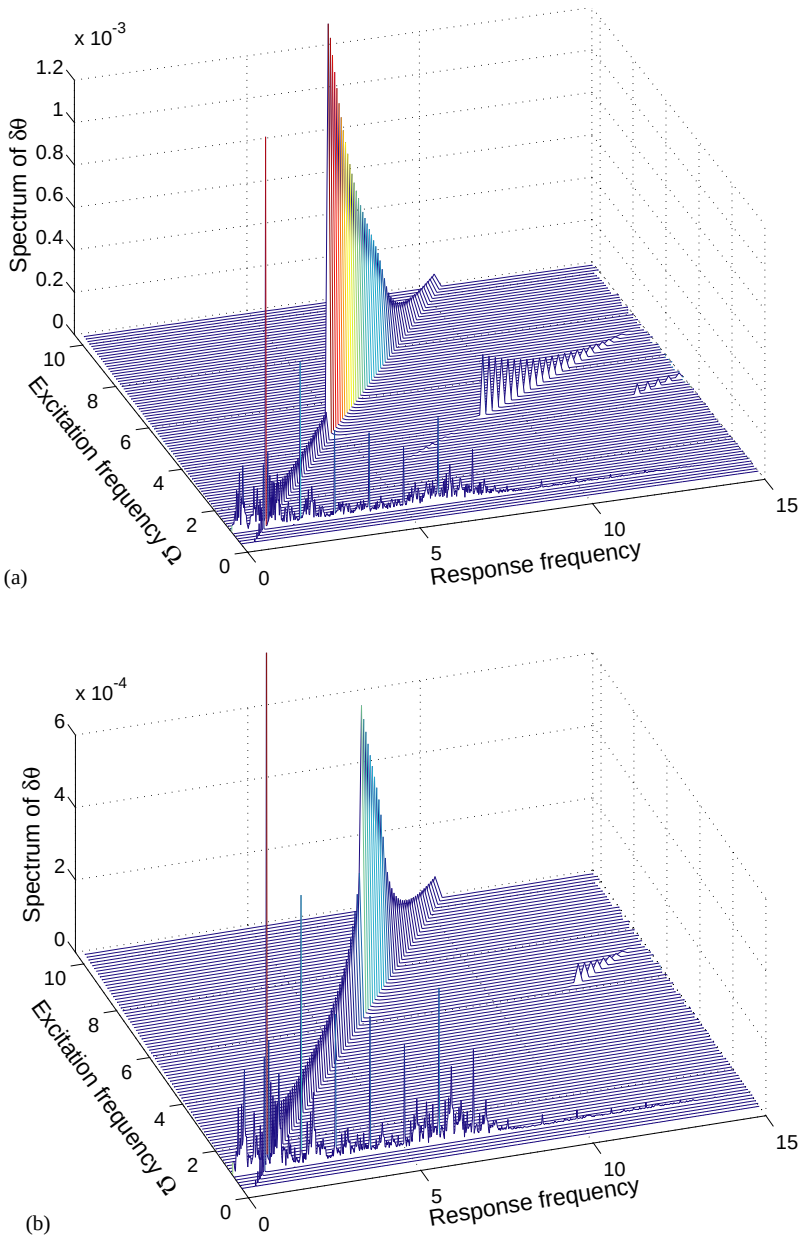

Fig. 6. Waterfall spectra of $\delta\theta$ using numerical integration and the parameter values from Table 1: (a) decreasing excitation frequency; (b) increasing excitation frequency.

sinusoidal, response due to the presence of non-linearity. The presence of these higher harmonics demonstrates the non-linear clutch disengagement outside the region of multiple solutions. Fig. 7(a) shows the time history and clutch torque for $\Omega = 4.455$, which lies at the point of local maximum response for decreasing frequency. Clutch disengagement (once per cycle) is apparent from the zero clutch torque.

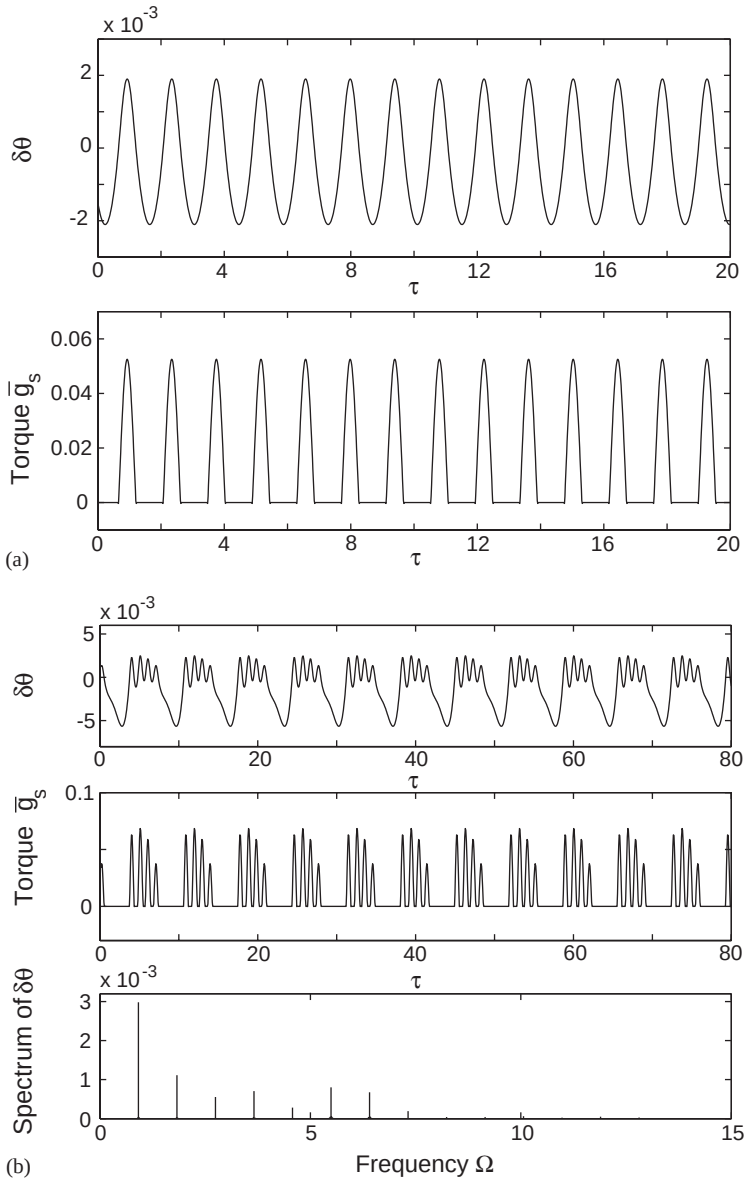

Fig. 7. (a) Time history of $\delta\theta$ and clutch spring torque $\bar{g}_s(\delta\theta)$ at $\Omega = 4.455$; (b) time history of $\delta\theta$, clutch spring torque $\bar{g}_s(\delta\theta)$ and spectrum of $\delta\theta$ at $\Omega = 0.915$. Results from numerical integration and decreasing frequency with parameter values from Table 1.

Results in the range $\Omega = 0.89$–1.07 are more complicated as shown in the exploded figure in Fig. 5(b). In this range, only a few small sections are periodic. In the hysteretic range for Ω just above 0.89 (point M), however, solutions are periodic for both increasing and decreasing frequency, though clutch disengagement occurs only along the upper branch achieved for

decreasing frequency. Fig. 7(b) shows time response for $\Omega = 0.915$ (point F) on the periodic upper branch at the right boundary of the region where multiple steady state solutions exist. Notice multiple clutch disengagements occur in a single period. Throughout the range from E to A ($0.94 < \Omega < 1.07$), solutions are primarily quasiperiodic or chaotic with a few periodic exceptions indicated by the solid lines (discussed later). Chaotic response is evident in the rich response spectrum in this range for both increasing and decreasing frequency (Fig. 6). Fig. 8 shows time histories and clutch torque for the excitation frequencies $\Omega = 0.945$ (quasiperiodic) and $\Omega = 1$ (chaotic). For $\Omega = 0.945$, the spectrum consists of discrete components, the phase portrait is a banded attractor, and the Poincaré map is a closed curve; for $\Omega = 1$, the distributed spectrum, phase portrait, and Poincaré map indicate chaos.

Application of HBM with arclength continuation and AUTO provides a more complete picture of the dynamics for varying frequency. The model is Eq. (3) with the smoothing function (6). The unknown vector $\bar{\mathbf{u}}$ and elements of $\mathbf{J}$ in Eq. (15) are given by

$$\bar{\mathbf{u}} = \{\mathbf{u}^{\mathrm{T}} \;\; \Omega\}^{\mathrm{T}}, \tag{20}$$

$$\bar{\mathbf{K}} = \begin{bmatrix} \mathbf{A} + \bar{C}_{11}\mathbf{B} + \bar{K}_b\mathbf{I} & \bar{C}_{12}\mathbf{B} \\ \bar{C}_{21}\mathbf{B} & \alpha\mathbf{A} + \bar{C}_{22}\mathbf{B} \end{bmatrix}, \quad \frac{\partial \mathbf{d}}{\partial \mathbf{u}} = \mathbf{\Gamma} \begin{bmatrix} \dfrac{\partial \bar{\mathbf{g}}_s}{\partial \boldsymbol{\theta}_p} & -\dfrac{\partial \bar{\mathbf{g}}_s}{\partial \boldsymbol{\theta}_p} \\ -\dfrac{\partial \bar{\mathbf{g}}_s}{\partial \boldsymbol{\theta}_p} & \dfrac{\partial \bar{\mathbf{g}}_s}{\partial \boldsymbol{\theta}_p} \end{bmatrix} \mathbf{L}, \tag{21}$$

$$\frac{\partial \bar{\mathbf{g}}_s}{\partial \boldsymbol{\theta}_p} = \mathrm{diag}\left(\tfrac{1}{2}\bar{K}_d[\varepsilon \,\mathrm{sech}^2(\varepsilon\boldsymbol{\delta\theta}) \cdot \boldsymbol{\delta\theta} + 1 + \tanh(\varepsilon\boldsymbol{\delta\theta})]\right), \tag{22}$$

$$\frac{\partial \mathbf{E}}{\partial \Omega} = \begin{bmatrix} -2\Omega\mathbf{A}_0 + \bar{C}_{11}\mathbf{B}_0 & \bar{C}_{12}\mathbf{B}_0 \\ \bar{C}_{21}\mathbf{B}_0 & -\alpha 2\Omega\mathbf{A}_0 + \bar{C}_{22}\mathbf{B}_0 \end{bmatrix} \mathbf{u}. \tag{23}$$

Excellent agreement between HBM and numerical integration is apparent from Fig. 5. No differences appear in the second resonant region. Harmonic balance gives a more complete picture of the periodic solutions for $\Omega \approx \Omega_1$, however. Three lobes of periodic solutions occur on the left of the exploded view in Fig. 5(b). Each of these has a small region of stability at their top, but are otherwise unstable. One can trace the jump-up and jump-down sequence observed in numerical integration as indicated by the arrows. On frequency increase, a dramatic jump up occurs from L to F near $\Omega \approx 0.91$. For decreasing frequency, solutions jump from the maximum lobe to the intermediate one and finally to the single solution that exists for $\Omega \leqslant 0.89$. Across the range E–A ($0.94 < \Omega < 1.07$), a single unstable periodic solution exists, with the exception of a small interval C–B of stability. That interval can be construed as a fourth lobe. These findings are consistent with numerical integration, where quasiperiodic and chaotic solutions occur along interval E–A (with the exception of the small stable periodic solution interval C–B). While the shape of the first mode resonance in Fig. 5(b) suggests near linear response, that is not the case in shape (discussed above) nor amplitude as shown by the linear system response curve in Fig. 5(b). Similar comments apply to the second mode resonance.

To compare results with AUTO, it is most convenient to use the maximum values of θ_p and θ_a. We choose the maximum of θ_p within a period to make the comparison in Fig. 9 between HBM, AUTO, and numerical integration. Fig. 9(a) shows excellent agreement of the three methods.

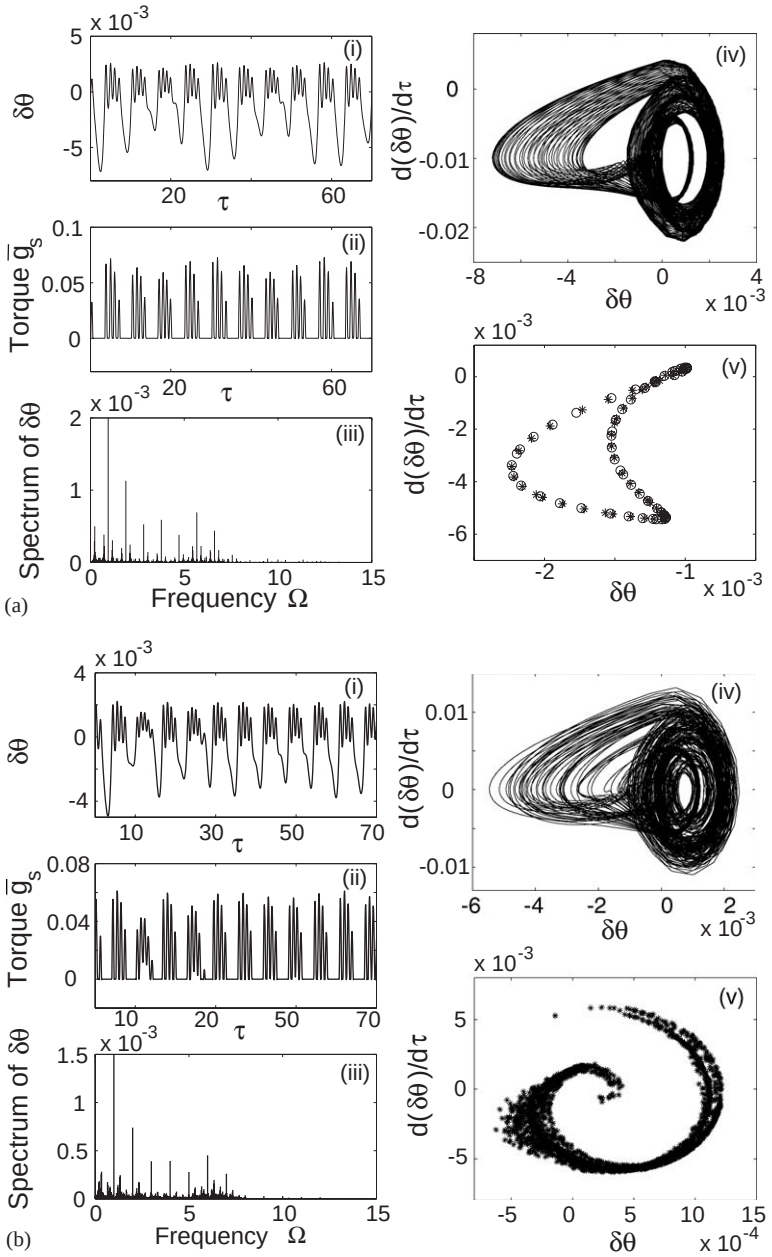

Fig. 8. (i) Time history of $\delta\theta$; (ii) clutch spring torque $\bar{g}_s(\delta\theta)$; (iii) spectrum of $\delta\theta$; (iv) phase diagram; (v) Poincaré map from numerical integration and decreasing frequency with parameter values from Table 1. (a) $\Omega = 0.945$; (b) $\Omega = 1$.

More detail is apparent in the zoomed regions of Fig. 9(b) and (c). (The letters A–M highlighting points in Fig. 9 correspond to the same points on Fig. 5(b).) Comparison between HBM and AUTO solutions is indistinguishable even in the details of Fig. 9(b) and (c) with the exception that

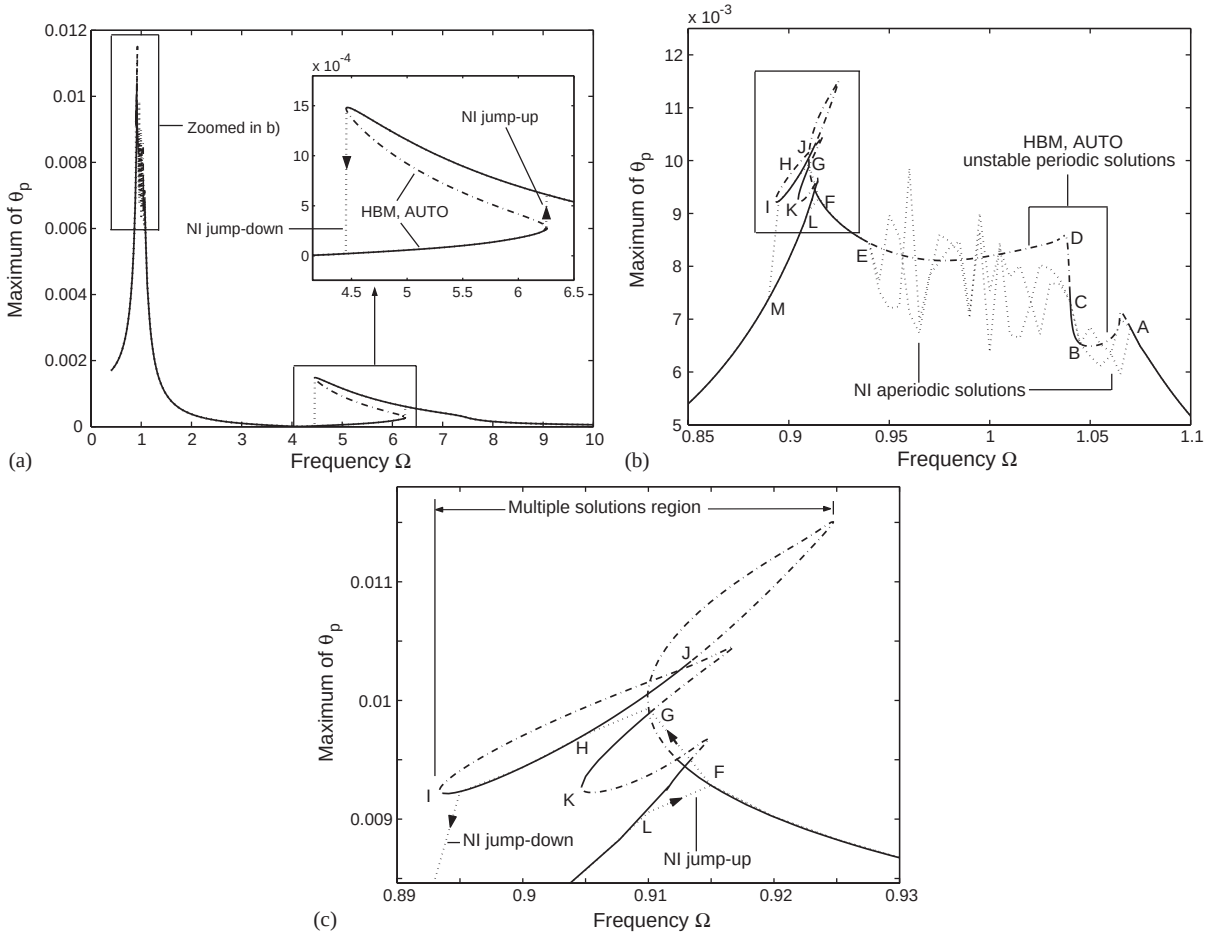

Fig. 9. Maximum of θ_p versus excitation frequency for parameters in Table 1. (a) Range of excitation frequencies including two resonances; (b) first resonant region; (c) zoom of the area highlighted in (b). HBM and AUTO stable (-), unstable (-·); NI (..).

HBM incorrectly predicts part of the branch F–G to be unstable. Increasing the number of harmonic terms and the temporal discretization resolution improves the results. In the region A–E, no stable periodic solutions exist, except for the small region B–C noted previously in Fig. 5(b). The numerical integration results confirm this conclusion. The pattern of jumps in the numerical integration results is consistent with the rich pattern of stable and unstable solution branches shown in Fig. 9(c) (with slight differences resulting from limited frequency resolution).

The impact of non-linearity is much different in the two resonant regimes $\Omega \approx \Omega_1, \Omega_2$. This stems from the difference in linear system vibration modes (Fig. 2). The second mode involves out-of-phase motion between the pulley and accessory shaft and is more prone to clutch disengagement. This non-linear softening spreads the resonance curve (and associated clutch disengagement) across a broad frequency range. The first mode generates less relative motion between pulley and accessory because these components move in-phase, so there is less softening non-linearity from

clutch disengagement. The frequency range over which disengagement occurs is markedly more limited. The amplitude is higher in the first mode resonant regime because the excitation from crankshaft fluctuations more directly excites this mode. At these high amplitudes, the system exhibits a rich range of bifurcations of periodic solutions not evident at the lower amplitudes near the second mode resonance.

4.2. Dependence on the clutch spring stiffness

In practice, the stiffness of the clutch spring can be designed across a wide range, and selected values are illustrated in Fig. 10. For finite stiffness, the term one-way decoupler is sometimes used. The change in linear system natural frequencies with $\bar{K}_d$ is shown in Fig. 11. Only the second mode natural frequency changes meaningfully because this mode is the only one with significant relative pulley/accessory motion (Fig. 2). The frequency response for various $\bar{K}_d$ is shown in Fig. 12 as computed by numerical integration. From the exploded inset, the amplitude of non-linear response for $\Omega \approx \Omega_1$ is relatively insensitive to $\bar{K}_d$ except for very low values, as one would expect from Fig. 11. Most solutions in this range are aperiodic, as discussed previously. An additional curve is shown in Fig. 12 for the s.d.o.f. system with a locked clutch (typical belt drive pulley). For $\Omega \approx \Omega_1$, the resonant response decreases significantly because of the one-way clutch non-linearity. The penalty balancing this benefit is the additional resonance region for $\Omega \approx \Omega_2$, much like a vibration absorber. The amplitude of response for $\Omega \approx \Omega_2$ is generally much lower than that for $\Omega \approx \Omega_1$, however. This amplitude decreases monotonically with increasing $\bar{K}_d$, and is negligible for $\bar{K}_d = 276.6$. In contrast, the amplitude for $\Omega \approx \Omega_1$ increases with increasing $\bar{K}_d$, though the changes are minimal compared to amplitude reductions for $\Omega \approx \Omega_2$. For the

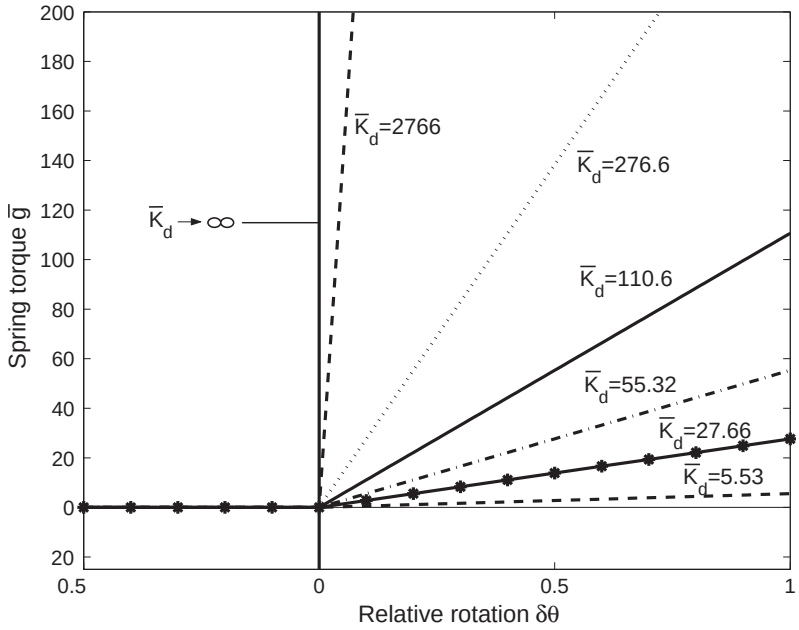

Fig. 10. Clutch spring torque for various spring stiffnesses $\bar{K}_d$.

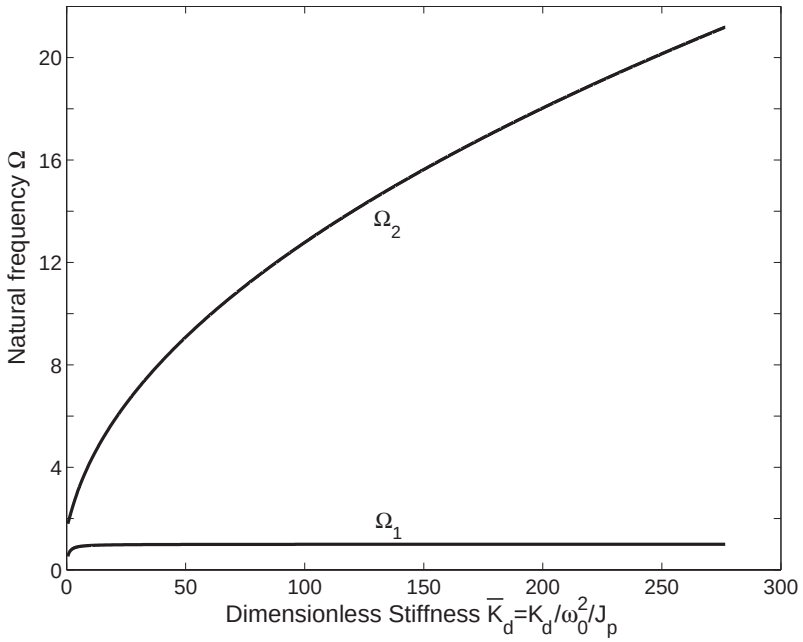

Fig. 11. Sensitivity of the linear system natural frequencies to clutch stiffness $\bar{K}_d$ for parameters in Table 1.

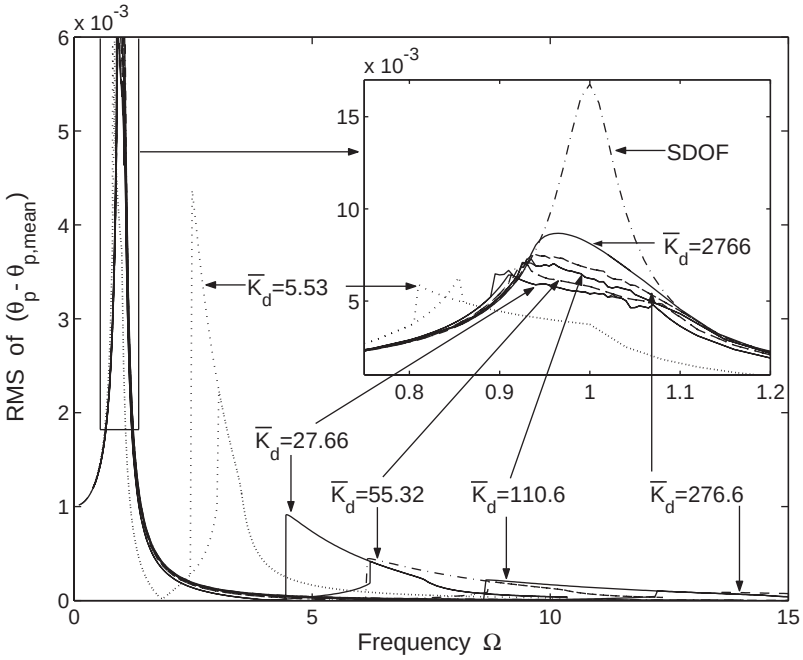

Fig. 12. The r.m.s. of $\theta_p - \theta_{p,mean}$ depending on spring stiffness $\bar{K}_d$ for parameter values of Table 1 by numerical integration using step function for the clutch torque (see Eq. (4)).

infinite stiffness limit as approximated by $\bar{K}_d = 2766$, the amplitude for $\Omega \approx \Omega_1$ is higher and noticeably smoother than for lower $\bar{K}_d$; solutions in this range are periodic. These results suggest use of large but not rigid clutch spring stiffness, although the optimal solution depends on the anticipated excitation frequency range. Both options are superior to the s.d.o.f. (no clutch) case.

To apply HBM, the unknown in Eq. (14) is $\bar{\mathbf{u}} = \{\mathbf{u}^{\mathrm{T}} \;\; \bar{K}_d\}^{\mathrm{T}}$. Under the assumption that the damping matrix $\bar{\mathbf{C}}$ is the same as for the nominal case, determination of the Jacobian matrix in Eq. (15) requires

$$\frac{\partial \mathbf{E}}{\partial \bar{K}_d} = \frac{\partial \mathbf{d}}{\partial \bar{K}_d} = \mathbf{\Gamma} \begin{Bmatrix} \dfrac{\partial \bar{\mathbf{g}}_s}{\partial \bar{K}_d} \\ -\dfrac{\partial \bar{\mathbf{g}}_s}{\partial \bar{K}_d} \end{Bmatrix}, \tag{24}$$

where $(\partial \bar{\mathbf{g}}_s / \partial \bar{K}_d) = \frac{1}{2}[1 + \tanh(\varepsilon \boldsymbol{\delta\theta})] \cdot \boldsymbol{\delta\theta}$. This procedure yields results that agree with Fig. 12 to the same degree as the comparison in Fig. 9.

4.3. Dependence on excitation amplitude

Now consider the influence of excitation amplitude A_m, which in a belt drive represents the magnitude of the crankshaft pulley fluctuations due to engine firing. The above results are for $A_m = 0.001$. When varying amplitude A_m for given excitation frequency Ω, the unknown in (14) is $\bar{\mathbf{u}} = \{\mathbf{u}^{\mathrm{T}} \;\; A_m\}^{\mathrm{T}}$. Eqs. (21) and (22) are again used to determine the Jacobian matrix (15) with the modification that Eq. (23) is replaced by

$$\frac{\partial \mathbf{E}}{\partial A_m} = -\frac{\partial \mathbf{F}}{\partial A_m} = -\{0 \;\; \beta \bar{K}_b \;\; 0 \;\; \cdots \;\; 0\}^{\mathrm{T}}_{2(2R+1)}. \tag{25}$$

Fig. 13(a) and (b) show the maximum of θ_p for varying A_m and other parameters as in Table 1 for three excitation frequencies $\Omega = 0.92, 1, 2$ determined by HBM and AUTO (the two results are indistinguishable). $\Omega = 0.92$ and $\Omega = 1$ are near resonant excitation frequencies for the first mode; $\Omega = 2$ is off-resonant. For $A_m > 0.007$, all periodic solutions are unstable except for a branch from $0.01 < A_m < 0.022$ for $\Omega = 1$. Note that for large excitation amplitudes the off-resonant periodic solution, while unstable, is higher amplitude than those for $\Omega = 0.92, 1$. Fig. 13(b) zooms the low excitation amplitude region of Fig. 13(a). Here the stable and unstable resonant amplitudes exceed the off-resonant one at $\Omega = 2$. A linear region is apparent for small A_m. With $A_m = 0.001$, the single periodic solution for $\Omega = 1$ is unstable, but there is a stable periodic solution for $\Omega = 0.92$, which is in agreement with Fig. 9(b). The cases for $\Omega = 6$ and 6.8 (Fig. 13(c)) exhibit the classical non-linear behavior. For $A_m = 0.001$, there are three solutions for $\Omega = 6$. Two are stable and the intermediate one is unstable. For $\Omega = 6.8$ only one solution is generated at all amplitudes. For large amplitudes, the single periodic solution branches for each of $\Omega = 6, 6.8$ are unstable and no stable periodic solutions exist.

4.4. Dependence on the ratio of pulley and accessory inertias

The parameter $\alpha = J_a/J_p$ governs the ratio of the inertia of the pulley to that of the accessory. Fig. 14 shows the sensitivity of the linear system natural frequencies to α. Fig. 15

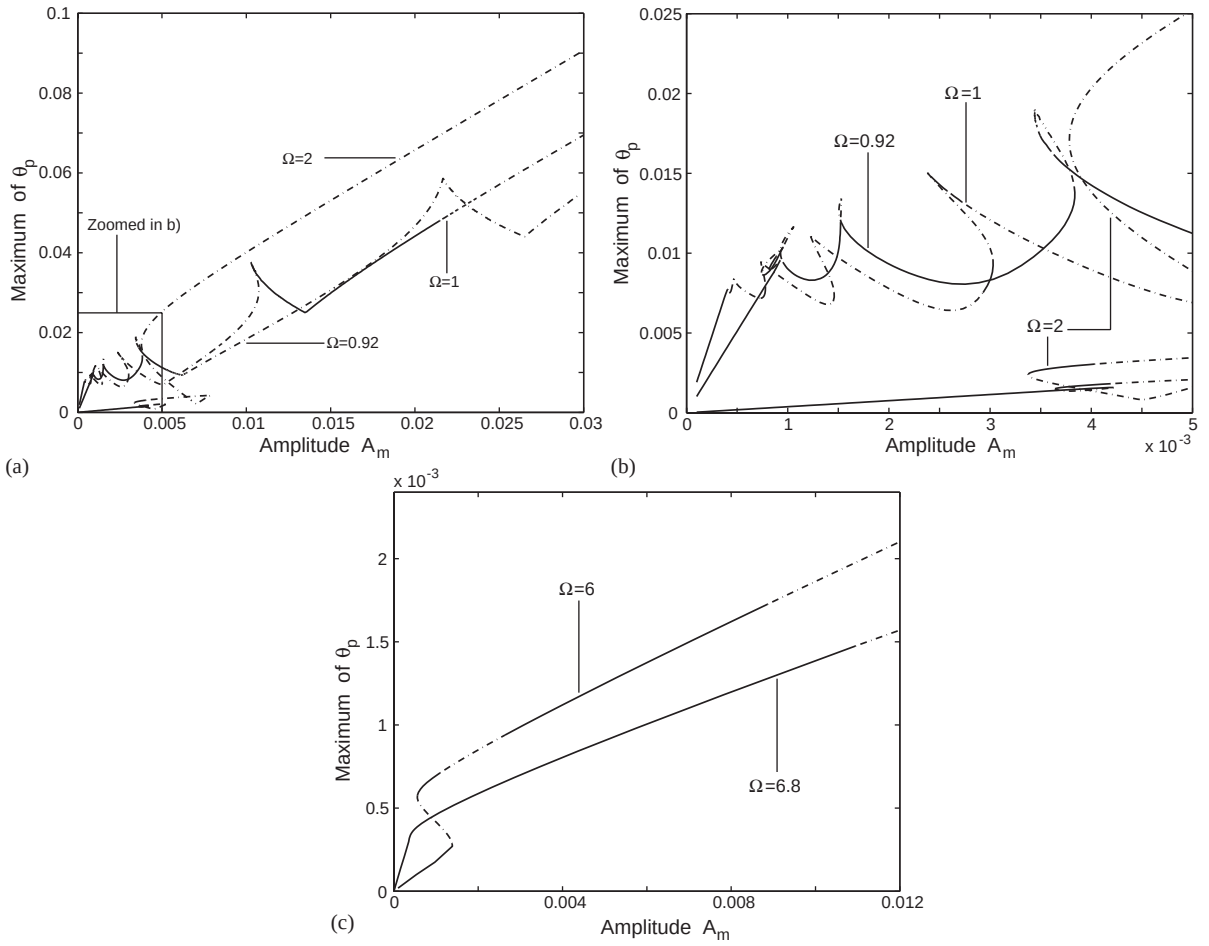

Fig. 13. Maximum of θ_p versus excitation amplitude for parameters in Table 1: (a) $\Omega = 0.92, 1, 2$; (b) zoomed plot of highlighted area in (a); (c) $\Omega = 6, 6.8$. HBM and AUTO stable (-), unstable (-·).

illustrates two excitation frequency sweep examples for $\alpha = 5$ and 0.3; $\alpha = 1.62$ is in Fig. 9. The results from HBM and AUTO are identical. For $\alpha = 5$, the inertia of the pulley is much smaller than that of the accessory, and the natural frequencies of the linear system are $\Omega_1 = 0.640$ and $\Omega_2 = 5.950$. At the second resonant peak, there is only one stable periodic solution branch at the bottom, and the two upper branches all consist of unstable periodic solutions except a small section close to the tip of the peak. This contrasts with $\alpha = 1.62$ in Fig. 9, where the upper branch at the second resonant region is always stable. Complex behavior near $\Omega_1 = 0.640$ is shown in the inset to Fig. 15. For $\alpha = 0.3$, the natural frequencies are $\Omega = 1.42$ and 11. The peak in the first mode is much more pronounced than the barely evident peak at $\Omega = 11$. All periodic solutions are stable except in a narrow region at the tip of the first peak.

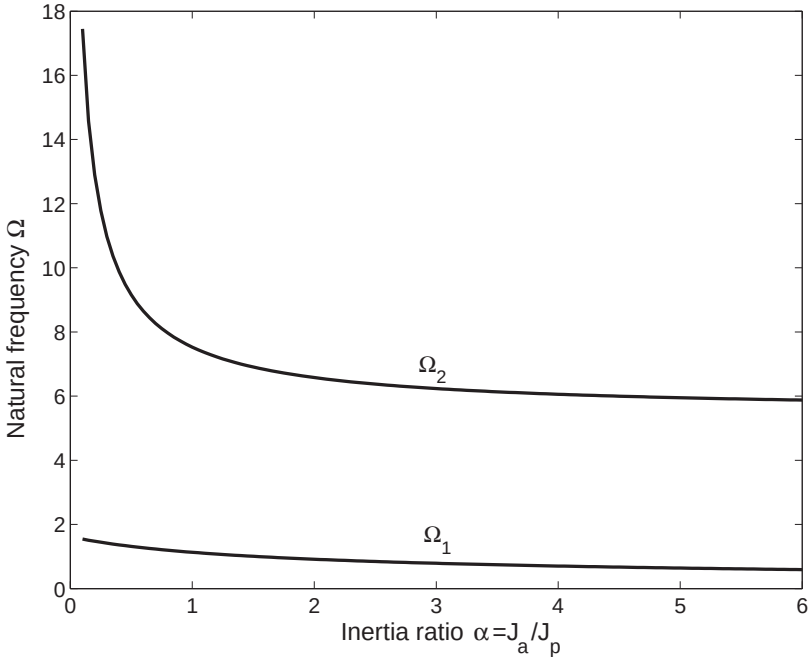

Fig. 14. Sensitivity of natural frequencies of linear system to α for parameters in Table 1.

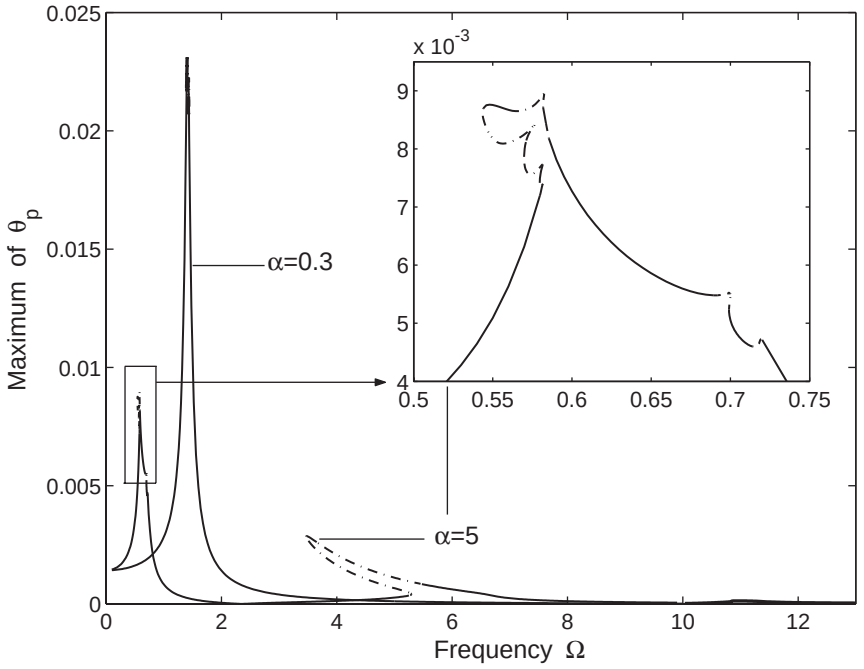

Fig. 15. Maximum of θ_p versus frequency for $\alpha = 5$ and $\alpha = 0.3$ with other parameters in Table 1. HBM and AUTO stable (-), unstable (-·).

Physically, imagine the case of a big pulley driving a small accessory, i.e., α is small. In this case, the non-linear clutch and accessory attached to the pulley have little impact on the belt–pulley system, and the behavior is largely that of a linear s.d.o.f. system. For larger α ($\alpha = 1.62$ in Fig. 9, $\alpha = 5$), considerably more pulley/accessory coupling occurs. Significant clutch disengagement occurs in the second, out-of-phase mode. The large amplitude response in the first mode creates a complicated periodic solution picture for $\Omega \approx \Omega_1$ even though this in-phase mode is less prone to disengagement.

5. Summary and conclusions

The non-linear dynamics of a two-pulley belt system with a one-way clutch are examined using a two-degree of freedom model. The non-linear one-way clutch is modelled as a spring with discontinuous stiffness, where clutch torque acts only for positive relative motion between the pulley and the accessory shaft. The problem is studied with three methods: multi-term harmonic balance, numerical integration, and the bifurcation software AUTO. All yield results with excellent agreement. Harmonic balance and AUTO yield the stable and unstable periodic solutions. Numerical integration gives details of the quasiperiodic and chaotic solutions that occur in the absence of stable periodic solutions. The main conclusions are

- The non-linear spring changes the s.d.o.f. system (no clutch) into a two-d.o.f. system, much like a vibration absorber. The frequency response is concentrated at two resonant regions near the natural frequencies of the two-d.o.f. linear model (clutch engaged). Significant softening non-linearity occurs due to clutch disengagement at the second natural frequency where the mode involves out-of-phase pulley–accessory motion. The clutch markedly decreases resonant amplitude near the first mode natural frequency, as it is designed to do. Near this region, a complicated pattern of periodic solution bifurcations occurs. Across a range of speeds, aperiodic, quasiperiodic and chaotic responses occur. Multiple disengagements per cycle occur in some periodic solutions.
- The stiffness of the clutch spring impacts the response considerably. Smaller values tend to minimize the response in the first (in-phase) mode. Larger values tend to minimize response in the second (out-of-phase) mode and simultaneously push this resonance to frequencies that may lie outside the range of practical importance. Large values reduce or eliminate the range in which chaotic or aperiodic solutions occur.
- Steady state solutions for large and small excitation amplitudes A_m at frequencies near the first mode resonance show a complex assortment of multiple stable/unstable periodic and aperiodic solutions. Calculation of closed-form approximations to these solution curves appears very difficult. Behavior near the second (out-of-phase) mode follows the classical softening non-linearity pattern similar to Duffing's equation, for example.
- The dynamics are sensitive to the inertia ratio $\alpha = J_a/J_p$ largely because this changes the nature of the vibration modes. For small α, or a large driven pulley attached to a small accessory, linear behavior dominates the system dynamics at the first resonance and the second mode resonance is hardly excited. With increasing accessory inertia, the modal force applied to the second mode increases, causing more disengagement in this out-of-phase mode and therefore

softening non-linearity; the dynamics of the first mode also show much more non-linear behavior.

Acknowledgements

The authors are grateful to Mark IV Automotive/Dayco Corporation for the support, to Dr. Björn Sandstede for providing guidance on the usage of the software AUTO, and to Mr. Gang Liu for some help developing the code for HBM algorithm.

References

[1] R. King, R. Monahan, Alternator pulley with integral overrunning clutch for reduction of belt noise, *1999 SAE International Congress and Exposition*, Detroit, MI, 1–4 March, 1999.
[2] P. Solfrank, P. Kelm, *The Dynamic Simulation of Automobile Accessory Drives*, 1999. http://www.ina.de.
[3] R.S. Beikmann, N.C. Perkins, A.G. Ulsoy, Free vibration of serpentine belt drive systems, *Journal of Vibration and Acoustics* 118 (1996) 406–413.
[4] S.-J. Hwang, N.C. Perkins, A.G. Ulsoy, R.J. Meckstroth, Rotational response and slip prediction of serpentine belt drive systems, *Journal of Vibration and Acoustics* 116 (1994) 71–78.
[5] L. Kong, R.G. Parker, Equilibrium and belt–pulley vibration coupling in serpentine belt drives, *American Society of Mechanical Engineers Journal of Applied Mechanics* 70 (2003) 739–750.
[6] L. Kong, R.G. Parker, Coupled belt–pulley vibration in serpentine drives with belt bending stiffness, *American Society of Mechanical Engineers Journal of Applied Mechanics* 71 (2004) 109–119.
[7] R.G. Parker, Efficient eigensolution, dynamic response, and eigensensitivity of serpentine belt drives, *Journal of Sound and Vibration* 270 (2004) 15–38.
[8] R.K. Jha, Modeling of High Speed Serpentine Belt Drive Systems and Spatial Discretization of Axially Moving Media Vibration Problems, Masters Thesis, The Ohio State University, 2000.
[9] P. Vernay, G. Ferraris, A. Delbez, P. Ouplomb, Transient behaviour of a sprag-type over-running clutch: an experimental study, *Journal of Sound and Vibration* 248 (3) (2001) 567–572.
[10] M.J. Leamy, T.M. Wasfy, Transient and steady-state dynamic finite element modeling of belt-drives, *Journal of Dynamic Systems, Measurement, and Control* 124 (2002) 575–581.
[11] E.J. Doedel, A.R. Champneys, T.F. Fairgrieve, Y.A. Kuznetsov, B. Sandstede, X. Wang, Auto97: continuation and bifurcation software for ordinary differential equations (with Homcont), Technical Report, Concordia University, 1997.
[12] G.W. Blankenship, A. Kahraman, Steady state forced response of a mechanical oscillator with combined parametric excitation and clearance type non-linearity, *Journal of Sound and Vibration* 185 (5) (1995) 743–765.
[13] M.J. Leamy, N.C. Perkins, Nonlinear periodic response of engine accessory drives with dry friction tensioners, *Journal of Vibration and Acoustics* 120 (1998) 909–916.
[14] C. Padmanabhan, R. Singh, Analysis of periodically excited non-linear systems by a parametric continuation technique, *Journal of Sound and Vibration* 184 (1) (1995) 35–58.
[15] A. Raghothama, S. Narayanan, Bifurcation and chaos in geared rotor bearing system by incremental harmonic balance method, *Journal of Sound and Vibration* 226 (3) (1999) 469–492.
[16] G. Von Groll, D.J. Ewins, The harmonic balance method with arc-length continuation in rotor/stator contact problems, *Journal of Sound and Vibration* 241 (2) (2001) 223–233.
[17] G.R. Baker, E.A. Overman, The Art of Scientific Computing, Draft, 2000.
[18] A.Y.T. Leung, S.K. Chui, Non-linear vibration of coupled Duffing oscillators by an improved incremental harmonic balance method, *Journal of Sound and Vibration* 181 (4) (1995) 619–633.
[19] K.B. Blair, C.M. Krousgrill, T.N. Farris, Harmonic balance and continuation techniques in the dynamic analysis of Duffing's equation, *Journal of Sound and Vibration* 202 (5) (1997) 717–731.

[20] P. Friedmann, C.E. Hammond, T.H. Woo, Efficient numerical treatment of periodic systems with application to stability problems, *International Journal of Numerical Methods in Engineering* 11 (1977) 1117–1136.
[21] C.S. Hsu, On approximating a general linear periodic system, *Journal of Mathematical Analysis and Application* 45 (1974) 234–251.
[22] C.S. Hsu, W.H. Cheng, Applications of the theory of impulsive parametric excitation and new treatments of general parametric excitation problems, *American Society of Mechanical Engineers Journal of Applied Mechanics* 40 (1973) 78–86.